N O T I C E

THIS DOCUMENT HAS BEEN REPRODUCED FROM MICROFICHE. ALTHOUGH IT IS RECOGNIZED THAT CERTAIN PORTIONS ARE ILLEGIBLE, IT IS BEING RELEASED IN THE INTEREST OF MAKING AVAILABLE AS MUCH INFORMATION AS POSSIBLE

NASA Technical Memorandum 81647

Elastohydrodynamic Lubrication of Elliptical Contacts

Bernard J. Hamrock
Lewis Research Center
Cleveland, Ohio

Lecture prepared for the
First Symposium INTERTRIBO '81
Štrbské Pleso, Czechoslovakia, April 27-29, 1981

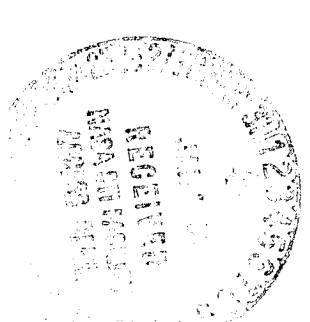

NASA

HAMROCK, B. J., B.S., M.S., and Ph.D.
NASA Lewis Research Center, U.S.A.

ELASTOHYDRODYNAMIC LUBRICATION OF ELLIPTICAL CONTACTS

Summary

The emphasis of the first part of the lecture is on fully flooded, elastohydrodynamically lubricated, elliptical contacts. A fully flooded conjunction is one in which the film thickness is not significantly changed when the amount of lubricant is increased. The relevant equations used in the elastohydrodynamic lubrication (EHL) of elliptical contacts are briefly described. The most important practical aspect of the elastohydrodynamic theory is the determination of the minimum film thickness within the contact. The maintenance of a fluid film of adequate magnitude is an essential feature of the correct operation of lubricated machine elements. The results to be presented show the influence of contact geometry on minimum film thickness as expressed by the ellipticity parameter and the dimensionless speed, load, and materials parameters. Film thickness equations are developed for materials of high elastic modulus, such as metal, and for materials of low elastic modulus, such as rubber. The solutions for materials of high elastic modulus are sometimes referred to as "hard EHL," and the solutions for materials of low elastic modulus as "soft EHL." In addition to the film thickness equations that are developed, plots of pressure and film thickness are presented. These theoretical solutions for film thickness have all the essential features of previously reported experimental observations based on optical interferometry.

In the second part of the lecture a theoretical study of the influence of lubricant starvation on film thickness and pressure in hard and soft elliptical elastohydrodynamic contacts is presented. From the results for both hard and soft EHL contacts a simple and important dimensionless inlet boundary distance is specified. This inlet boundary defines whether a fully flooded or a starved condition exists in the contact. It is also found that the film thickness for a starved condition can be written in dimensionless terms as a function of the inlet distance parameter and the film thickness for a fully flooded condition. Contour plots of pressure and film thickness in and around the contact are shown for fully flooded and starved conditions. The theoretical findings are compared directly with results obtained experimentally.

1. Introduction

Elastohydrodynamic lubrication is a form of fluid-film lubrication where elastic deformation of bearing surfaces becomes significant. It is usually associated with highly stressed machine components of low conformity, such as gears and rolling-element bearings. This lubrication mechanism is also encountered with soft bearing materials, such as rubber seals and tires. The common factor in these applications is that local elastic deformation of the solids provides coherent fluid films and thus asperity interaction is prevented.

Historically, elastohydrodynamic lubrication may be viewed as one of the major developments in the field of tribology in the twentieth century. It not only revealed the existence of a previously unsuspected regime of lubrication in highly stressed and nonconformal machine elements, such as gears and rolling-element bearings, but it brought order to the understanding of the complete spectrum of lubrication ranging from boundary to hydrodynamic.

2. Conformal and Nonconformal Surfaces

Hydrodynamic lubrication is generally characterized by surfaces that are conformal. That is, the surfaces fit snugly into each other with a high degree of geometrical conformity, so that the load is carried over a relatively large area. Furthermore the load-carrying surface area remains essentially constant while the load is increased. Fluid-film journal and slider bearings exhibit conformal surfaces. In journal bearings the radial clearance between the shaft and the bearing is typically one-thousandth of the shaft diameter; in slider bearings the inclination of the bearing surface to the runner is typically one part in a thousand.

Many machine elements have contacting surfaces that do not conform to each other very well. The full burden of the load must then be carried by a very small contact area. In general the contact areas between nonconformal surfaces enlarge considerably with increasing load but are still small compared with the contact areas between conformal surfaces. Some examples of these nonconformal surfaces are mating gear teeth, cams and followers, and rolling-element bearings.

The load per unit area in conformal bearings is relatively low, typically only 1 MN/m^2 and seldom over 7 MN/m^2. By contrast, the load per unit area in nonconformal contacts, such as those that exist in ball bearings, will generally exceed 700 MN/m^2, even at modest applied loads. These high pressures result in elastic deformation of materials such that the elliptical contact areas are formed for oil film generation and load support.

The significance of the high contact pressures is that they result in a considerable increase in fluid viscosity. Inasmuch as viscosity is a measure of a fluid's resistance to flow, this increase greatly enhances the lubricant's ability to support load without being squeezed out of the contact zone.

The undeformed geometry of contacting solids can be represented in general terms by two ellipsoids. The two solids with different radii of curvature in a pair of principal planes (x and y) passing through the contact between the solids make contact at a single point under the condition of zero applied load. Such a condition is called point contact and is shown in figure 1, where the radii of curvature are denoted by r's. It is assumed throughout the lecture that convex surfaces, as shown in figure 1, exhibit positive curvature and concave surfaces, negative curvature. Therefore, if the center of curvature lies within the solid, the radius of curvature is positive; if the center of curvature lies outside the solid, the radius of curvature is negative. It is important to note that if coordinates x and y are chosen such that

$$\frac{1}{r_{ax}} + \frac{1}{r_{bx}} > \frac{1}{r_{ay}} + \frac{1}{r_{by}} \tag{1}$$

coordinate x then determines the direction of the semiminor axis of the contact area when a load is applied and y, the direction of the semimajor axis.

3. Relevant Equations

The relevant equations used in elastohydrodynamic lubrication of elliptical contacts are as follows:

Lubrication equation (Reynolds equation)

$$\frac{\partial}{\partial x}\left(\frac{\rho h^3}{\eta}\frac{\partial p}{\partial x}\right) + \frac{\partial}{\partial y}\left(\frac{\rho h^3}{\eta}\frac{\partial p}{\partial y}\right) = 12u\frac{\partial}{\partial x}(\rho h) \tag{2}$$

where $$u = \frac{u_a + u_b}{2}$$

Viscosity variation

$$\eta = \eta_0 e^{\alpha p} \tag{3}$$

where η_0 is the coefficient of absolute or dynamic viscosity at atmospheric pressure and α is the pressure-viscosity coefficient of the fluid.

Density variation (for mineral oils)

$$\rho = \rho_0\left(1 + \frac{0.6\,p}{1 + 1.7\,p}\right) \tag{4}$$

where ρ_0 is the density at atmospheric conditions.

Elasticity equation

$$w = \frac{2}{E'}\iint_A \frac{p(x,y)\,dA}{\sqrt{(x - x_1)^2 + (y - y_1)^2}} \tag{5}$$

where

$$E' = \frac{2}{\left(\frac{1 - \nu_a^2}{E_a} + \frac{1 - \nu_b^2}{E_b}\right)} \tag{6}$$

Film thickness equation

$$h = h_0 + S(x,y) + w(x,y)$$

$$= h_0 + \frac{x^2}{2R_x} + \frac{y^2}{2R_y} + w(x,y) \tag{7}$$

where $$\frac{1}{R_x} = \frac{1}{r_{ax}} + \frac{1}{r_{bx}} \tag{8}$$

$$\frac{1}{R_y} = \frac{1}{r_{ay}} + \frac{1}{r_{by}} \tag{9}$$

The problem is to calculate the pressure distribution in the contact and at the same time allow for the effects that this pressure will have on the properties of the fluid and on the geometry of the elastic solids. The solution will also provide the shape of the lubricant film, particularly the minimum clearance between the solids. A detailed description of the elasticity model used is given in Dowson and Hamrock (1976), and the complete EHL theory is given in Hamrock and Dowson (1976).

4. Dimensionless Grouping

The variables resulting from the isothermal elliptical contact theory developed in Hamrock and Dowson (1976) are

- E' effective elastic modulus, N/m^2
- F normal applied load, N
- h film thickness, m
- R_x effective radius in x (motion) direction, m
- R_y effective radius in y (transverse) direction, m
- u mean surface velocity in x direction, m/s
- α pressure-viscosity coefficient of fluid, m^2/N
- η_0 atmospheric viscosity, N s/m^2

From these variables the following five dimensionless groupings were established:

Dimensionless film thickness

$$H = \frac{h}{R_x} \tag{10}$$

Ellipticity parameter

$$k = \frac{a}{b} = 1.03\left(\frac{R_y}{R_x}\right)^{0.64} \tag{11}$$

Brewe and Hamrock (1977) used a linear regression by the method of least squares to obtain the simplified equations given in equation (11). That is, for given sets of pairs of data $\{[k_j, (R_y/R_x)_j], j = 1, 2, \ldots, n\}$, a power fit using a linear regression by the method of least squares resulted in obtaining equation (11).

Dimensionless load parameter

$$W = \frac{F}{E' R_x^2} \tag{12}$$

Dimensionless speed parameter

$$U = \frac{\eta_0 u}{E' R_x} \tag{13}$$

Dimensionless materials parameter

$$G = \alpha E' \tag{14}$$

The dimensionless film thickness can thus be written as a function of the other four parameters

$$H = f(k, U, W, G) \tag{15}$$

The influence of the dimensionless parameters k, U, W, and G on minimum film thickness H_{min} is presented later for both hard and soft contacts.

The set of dimensionless groups $\{H, k, U, W, G\}$ is a useful collection of parameters for evaluating the results presented in this lecture. It is also comparable to the set of dimensionless parameters used in the initial elastohydrodynamic analysis of line contacts, and it has the merit that the physical significance of each term is readily apparent. However, a number of authors, for example, Moes (1965 66) and Theyse (1966), have noted that this set of dimensionless groups can be reduced by one parameter without any loss of generality.

5. Fully Flooded Hard-EHL Results

By using the numerical procedures outlined in Hamrock and Dowson (1976) the influence of the ellipticity parameter and the dimensionless speed, load, and materials parameters on minimum film thickness has been investigated for hard-EHL, fully flooded contacts (Hamrock and Dowson, 1977b). The ellipticity parameter k was varied from 1 (a ball-on-plate configuration) to 8 (a configuration approaching a rectangular contact). The dimensionless speed U was varied over a range of nearly two orders of magnitude, and the dimensionless load parameter W over a range of one order of magnitude. Situations equivalent to using solid materials of bronze, steel, and silicon nitride and lubricants of paraffinic and naphthenic oils were considered in an investigation of the role of the dimensionless materials parameter G. The 34 cases used to generate the minimum-film-thickness formula are given in table 1. In the table H_{min} corresponds to the minimum film thickness obtained from the EHL elliptical contact theory given in Hamrock and Dowson (1976). The minimum-film-thickness formula obtained from a least-squares fit of the data was first given in Hamrock and Dowson (1977b) and is given here as

$$\tilde{H}_{min} = 3.63\, U^{0.68} G^{0.49} W^{-0.073} (1 - e^{-0.68k}) \tag{16}$$

In table 1 $\tilde{H}_{min}$ is the minimum film thickness obtained from equation (16). The percentage difference between $\tilde{H}_{min}$ and H_{min} is expressed by

$$D_1 = \left(\frac{\tilde{H}_{min} - H_{min}}{H_{min}} \right) 100 \tag{17}$$

In table 1 the values of D_1 are within ±5 percent.

A representative contour plot of dimensionless pressure is shown in figure 2 for $k = 1.25$, $U = 0.168 \times 10^{-11}$, $W = 0.111 \times 10^{-6}$, and $G = 4522$. In this figure and in figure 3, the + symbol indicates the center of the Hertzian contact zone. The dimensionless representation of the X and Y coordinates causes the actual Hertzian contact ellipse to be a circle regardless of the value of the ellipticity parameter. The Hertzian contact circle is shown by asterisks. On the figure is a key showing the contour labels and each corresponding value of dimensionless pressure. The inlet region is to the left and the exit region is to the right. The pressure gradient at the exit end of the conjunction is much larger than that in the inlet region. In figure 2 a pressure spike is visible at the exit of the contact.

Contour plots of film thickness are shown in figure 3 for $k = 1.25$, $U = 0.168 \times 10^{-11}$, $W = 0.111 \times 10^{-6}$, and $G = 4522$. In this figure two minimum-film-thickness regions occur in well-defined side lobes that follow, and are close to, the edge of the Hertzian contact ellipse. These results reproduce all the essential features of previously reported experimental observations based on optical interferometry (Cameron and Gohar, 1966).

The variation of pressure and film thickness in the direction of rolling quite close to the X-axis near the midplane of the conjunction is shown in figure 4 for three values of U. The values of the dimensionless load, materials, and ellipticity parameters were held constant at $k = 6$, $W = 0.737 \times 10^{-6}$, and $G = 4522$. In figure 4(a) the dashed line corresponds to the Hertzian pressure distribution. This figure shows that the pressure at any location in the inlet region rises as the speed increases, a result that is also consistent with the elastohydrodynamic theory for line or rectangular contacts. Furthermore, as the speed decreases, the height of the pressure spike decreases and

the hydrodynamic pressures gradually approach the semielliptical form of the Hertzian contact stresses. Note that the location of the pressure spike moves downstream toward the edge of the Hertzian contact ellipse as the speed decreases. For nominal line or rectangular contacts Dowson and Higginson (1966) showed results similar to those in figure 4(a).

The typical elastohydrodynamic film shape with an essentially parallel section in the central region is shown in figure 4(b). There is little sign of a reentrant region in this case, except perhaps at the lowest speed. Also, there is a considerable change in the film thickness as the dimensionless speed is changed, as indicated by equation (16). This illustrates most clearly the dominant effect of the dimensionless speed parameter U on the minimum film thickness in elastohydrodynamic contacts.

The variation of pressure and film thickness in the direction of motion along a line close to the midplane of the conjunction is shown in figure 5 for three values of dimensionless load parameter. The values of the dimensionless speed, materials, and ellipticity parameters were held fixed at $U = 0.168\times10^{-11}$, $G = 4\times10^{3}$, and $k = 6$. Note from figure 5(a) that the pressure at any location in the inlet region falls as the load increases. For the highest load ($W = 1.10\times10^{-6}$), figure 5(b), the film thickness rises between the central region and the outlet restriction. This reentrant effect is attributed to lubricant compressibility. Note also that at $W = 0.5\times10^{-6}$ the film thickness is slightly smaller than at $W = 1.10\times10^{-6}$. This somewhat curious result is linked to the fact that the location of the minimum film thickness also changes drastically over this load range. At the lower load the minimum film thickness is located on the midplane of the conjunction downstream from the center of the contact; at the higher load it moves to the side lobes as described earlier.

e. Fully Flooded Soft-EHL Results

The earlier studies of elastohydrodynamic lubrication of conjunctions of elliptical form are applied to the particular and interesting situation exhibited by materials of low elastic modulus (soft EHL). The procedure used in obtaining the soft-EHL results is given in Hamrock and Dowson (1978). The ellipticity parameter was varied from 1 (a ball-on-plate configuration) to 10 (a configuration approaching a nominal line or rectangular contact). The dimensionless speed and load parameters were varied by one order of magnitude. Seventeen different cases used to generate the minimum-film-thickness formula are given in table II. In the table H_{min} corresponds to the minimum film thickness obtained from applying the EHL elliptical contact theory given in Hamrock and Dowson (1976) to the soft-EHL contacts. The minimum-film thickness formula obtained from a least squares fit of the data was first given in Hamrock and Dowson (1978) and is given here as

$$\left[\bar{H}_{min} = 7.43\, U^{0.65} W^{-0.21} \left(1 - 0.85\, e^{-0.31k}\right)\right] \tag{18}$$

In table II $\bar{H}_{min}$ is the minimum film thickness obtained from equation (18). The percentage difference between H_{min} and $\bar{H}_{min}$ is expressed by D_1, given in equation (17). The values of D_1 in table II are within the range -8 to 3 percent.

It is interesting to compare the equation for materials of low elastic modulus (soft EHL, eq. (18)) with the corresponding equation for materials of high elastic modulus (hard EHL) given in equation (16). The powers of U in equations (18) and (16) are similar, but the power of W is much more significant for low elastic-modulus materials. The expression showing the effect of the ellipticity parameter is of exponential form in both equations, but with different constants.

A major difference between equations (18) and (16) is the absence of a materials parameter G in the expression for low-elastic-modulus materials. There are two reasons for this. One is the negligible effect of pressure on the viscosity of the lubricating fluid, and the other is the way in which the role of elasticity is simply and automatically incorporated into the prediction of conjunction behavior through an increase in the size of the Hertzian contact zone corresponding to changes in load. As a check on the validity of this, case 9 of table II was repeated with the material changed from nitrile to silicone rubber. The results of this change are recorded as case 17 in table II. The dimensionless minimum film thickness calculated from the full numerical solution to the elastohydrodynamic contact theory was 181.8×10^{-6}, and the dimensionless minimum film thickness predicted from equation (18) turned out to be 182.5×10^{-6}. This clearly indicates a lack of dependence of the minimum film thickness for low-elastic-modulus materials on the materials parameter.

The variation of the ratio $H_{min}/H_{min,r}$ is shown in figure 6, where $H_{min,r}$ is the minimum film thickness for rectangular contacts, with the ellipticity parameter k for both high- and low-elastic-modulus materials. If it is assumed that the minimum film thickness obtained from the elastohydrodynamic analysis of elliptical contacts can only be obtained to an accuracy of 3 percent, we find that the ratio $H_{min}/H_{min,r}$ approaches the limiting

value at $k = 5$ for high-elastic-modulus materials. For low-elastic-modulus materials the ratio approaches the limiting value more slowly, but it is reasonable to state that the rectangular-contact solution will give a very good prediction of the minimum film thickness for conjunctions in which k exceeds about 11.

7. Fully Flooded - Starved Boundary

The computing area in and around the Hertzian contact is shown in figure 7. In this figure the coordinate X is made dimensionless with respect to the semiminor axis b of the contact ellipse, and the coordinate Y is made dimensionless with respect to the semimajor axis a of the contact ellipse. The ellipticity parameter k is defined as the semimajor axis divided by the semiminor axis of the contact ellipse ($k = a/b$). Because of the dimensionless form of the coordinates X and Y the Hertzian contact ellipse becomes a Hertzian circle regardless of the value of k. This Hertzian contact circle is shown in figure 7 with a radius of unity. The edges of the computing area, where the pressure is assumed to be ambient, are also denoted. In this figure the dimensionless inlet distance $\bar{m}$, which is equal to the dimensionless distance from the center of the Hertzian contact zone to the inlet edge of the computing area, is shown. Lubricant starvation can be studied by simply changing the dimensionless inlet distance $\bar{m}$. A fully flooded condition is said to exist when the dimensionless inlet distance ceases to influence the minimum film thickness to any significant extent.

The value at which the minimum film thickness first starts to change when $\bar{m}$ is gradually reduced from a fully flooded condition is called the fully flooded - starved boundary position and is denoted by m^*. Therefore lubricant starvation was studied by using the basic elastohydrodynamic lubrication elliptical contact theory developed earlier in the lecture and by observing how reducing the dimensionless inlet distance affected the basic features of the conjunction. The next two sections make extensive use of the work presented by Hamrock and Dowson (1977a) and Hamrock and Dowson (1979).

8. Starved Hard-EHL Results

Table III shows how changing the dimensionless inlet distance affected the dimensionless minimum film thickness for three groups of dimensionless load and speed parameters. All the data presented in this section are for hard-EHL contacts that have a materials parameter G fixed at 4500 and the ellipticity parameter, at 6. It can be seen from table III that, as the dimensionless inlet distance $\bar{m}$ decreases, the dimensionless minimum film thickness H_{min} also decreases.

Table IV shows how the three groups of dimensionless speed and load parameters considered affected the location of the dimensionless inlet boundary distance m^*. Also given in this table are the corresponding values of dimensionless central and minimum film thickness for the fully flooded condition as obtained by interpolating the numerical values. The value of the dimensionless inlet boundary position m^* shown in table IV was obtained by using the data from table III when the following equation was satisfied:

$$\frac{H_{min} - (H_{min})_{\bar{m}=m^*}}{H_{min}} = 0.03 \qquad (19)$$

The value of 0.03 was used in equation (19) since it was ascertained that the data in table III were accurate to only ±3 percent.

The general form of the equation that describes how the dimensionless inlet distance at the fully flooded - starved boundary m^* varies with the geometry and central film thickness of an elliptical elastohydrodynamic conjunction is given as

$$m^* - 1 = A^* \left[\left(\frac{R_x}{b} \right)^{c^*} H_{min} \right]^{B^*} \qquad (20)$$

The right side of equation (20) is similar in form to the equations given by Wolveridge, et al. (1971) and Wedeven, et al. (1971). By applying a least-squares power fit to the data obtained from table III we can write

$$\left| m^* = 1 + 3.34 \left[\left(\frac{R_x}{b} \right)^{c^*} H_{min} \right]^{0.56} \right| \qquad (21)$$

A fully flooded condition exists when $\bar{m} \geq m^*$, and a starved condition exists when $\bar{m} < m^*$.

Having clearly established the limiting location of the inlet boundary for the fully flooded conditions (eq. (21)) we can develop an equation defining the dimensionless film thickness for elliptical conjunctions operating under starved lubrication conditions. The ratio between the dimensionless minimum film thickness in starved and fully flooded conditions can be expressed in general form as

$$\frac{H_{min,s}}{H_{min}} = C^* \left(\frac{\bar{m} - 1}{m^* - 1} \right)^{D^*} \qquad (22)$$

Table V shows how the ratio of the dimensionless inlet distance parameter to the fully flooded - starved boundary $(\bar{m} - 1)/(m^* - 1)$ affects the ratio of minimum film thickness in the starved and fully flooded conditions $H_{min,s}/H_{min}$. A least-squares power curve fit to the 16 pairs of data points

$$\left[\left(\frac{H_{min,s}}{H_{min}}\right)_i, \left(\frac{\tilde{m} - 1}{m^* - 1}\right)_i\right], \qquad i = 1,2, \ldots, 16$$

was used in obtaining values for C^* and D^* in equation (22). For these values of C^* and D^* the dimensionless minimum film thickness for a starved condition can be written as

$$\boxed{H_{min,s} = H_{min}\left(\frac{\tilde{m} - 1}{m^* - 1}\right)^{0.25}} \qquad (23)$$

Therefore, whenever $\tilde{m} < m^*$, where m^* is defined by equation (21), a starved lubrication condition exists. When this is true, the dimensionless minimum film thickness is expressed by equation (23). If $\tilde{m} \geq m^*$, where m^* is defined by equation (21), a fully flooded condition exists. Expressions for the dimensionless minimum film thickness for a fully flooded condition H_{min} are given in equation (16).

Figures 8 to 11 explain more fully what happens in going from a fully flooded to a starved lubrication condition. As in the earlier part of the lecture the + symbol indicates the center of the Hertzian contact, and the asterisks indicate the Hertzian contact circle. Also on each figure the contour labels and each corresponding value are given.

In figures 8(a), (b), and (c) contour plots of dimensionless pressure ($P = p/p'$) are given for group 1 of table III and for dimensionless inlet distances $\tilde{m}$ of 4, 2, and 1.25, respectively. In these figures the contour values are the same in each plot. The pressure spikes are evident in figures 8(a) and (b), but no pressure spike appears in figure 8(c). This implies that as the dimensionless inlet distance $\tilde{m}$ decreases, or as the severity of lubricant starvation increases, the pressure spike is suppressed. Figure 8(a), with $\tilde{m} = 4$, corresponds to a fully flooded condition; figure 8(b), with $\tilde{m} = 2$, to a starved condition; and figure 8(c), with $\tilde{m} = 1.25$, to even more severe starvation. Once lubricant starvation occurs, the severity of the situation within the conjunction increases rapidly as $\tilde{m}$ is decreased and dry contact conditions are approached.

Contour plots of the dimensionless film thickness ($H = h/R_x$) for the results shown in group 1 of table III and for conditions corresponding to the three pressure distributions shown in figure 8 are reproduced in figure 9. It is clear that the film shape in the central region of the elastohydrodynamic conjunction becomes more parallel as lubricant starvation increases and that the region occupied by the minimum film thickness becomes more concentrated. Note also that the values attached to the film thickness contours for the starved condition (fig. 9(c)) are much smaller than those of the film thickness contours for the fully flooded condition (fig. 9(a)).

The application of optical interferometry allows the film thickness through the conjunction to be determined experimentally. An example of the interference pattern for a starved, elastohydrodynamically lubricated conjunction is shown in figure 10, which was kindly supplied by Sanborn from the work he reported in 1969. This technique produces information of great clarity and beauty. The film shape of the lubricated conjunction revealed by the experimental results shown in figure 10 compares quite well in qualitative terms with the theoretical results shown in figure 9(c).

9. Starved Soft-EHL Results

By using the theory and numerical procedure mentioned earlier in the lecture, we can investigate the influence of lubricant starvation on minimum film thickness in starved, elliptical, elastohydrodynamic conjunctions for low-elastic-modulus materials (soft EHL). Lubricant starvation is studied by simply moving the inlet boundary closer to the center of the conjunction, as described in the previous section.

Table VI shows how the dimensionless inlet distance affects the dimensionless film thickness for three groups of dimensionless load and speed parameters. For all the results presented in this section the dimensionless materials parameter G was fixed at 0.4276, and the ellipticity parameter k was fixed at 6. The results shown in table VI clearly indicate the adverse effect of lubricant starvation in the sense that, as the dimensionless inlet distance $\tilde{m}$ decreases, the dimensionless minimum film thickness H_{min} also decreases.

Table VII shows how the three groups of dimensionless speed and load parameters affect the limiting location of the dimensionless critical inlet boundary distance m^*. Also given in this table are corresponding values of the dimensionless minimum film thickness for the fully flooded condition, as obtained by interpolating the numerical values. By making use of table VI and following the procedure outlined in the previous section, we can write the critical dimensionless inlet boundary distance at which starvation becomes important for low-elastic-modulus materials as

$$\boxed{m^* = 1 + 1.07\left[\left(\frac{R_x}{b}\right)^2 \tilde{H}_{min}\right]^{0.16}} \qquad (24)$$

where $\tilde{H}_{min}$ is obtained from the fully flooded soft-EHL results in equation (18).

Table VIII shows how m^* affects the ratio of minimum film thickness in the starved and fully flooded conditions $\tilde{H}_{min,s}/H_{min}$. The dimensionless minimum film thickness for a starved condition

for low elastic modulus materials can thus be written as

$$\tilde{H}_{min,s} = H_{min}\left(\frac{\tilde{m}-1}{m^*-1}\right)^{0.22} \qquad (25)$$

Therefore, whenever $\tilde{m} < m^*$, where m^* is defined by equation (24), a lubricant starvation condition exists. When this is true, the dimensionless minimum film thickness is expressed by equation (25). If $\tilde{m} \geq m^*$, a fully flooded condition exists, and the expression for the dimensionless minimum film thickness for a fully flooded condition H_{min} for materials of low elastic modulus is given in equation (18).

10. References

Brewe, D. E. and Hamrock, B. J. (1977) "Simplified Solution for Elliptical Contact Deformation Between Two Elastic Solids," J. Lubr. Technol. 99 (4), 485-487.

Cameron, A. and Gohar, R. (1966) "Theoretical and Experimental Studies of the Oil Film in Lubricated Point Contact," Proc. R. Soc. (London) 291A (1427), 520-536.

Dowson, D. and Hamrock, B. J. (1976) "Numerical Evaluation of the Surface Deformation of Elastic Solids Subjected to a Hertzian Contact Stress." ASLE Trans. 19 (4), 279-286.

Dowson, D. and Higginson, G. R. (1966) Elasto-Hydrodynamic Lubrication - The Fundamentals of Roller and Gear Lubrication. Pergamon Press, Oxford.

Hamrock, B. J. and Dowson, D. (1976) "Isothermal Elastohydrodynamic Lubrication of Point Contacts. Part I - Theoretical Formulation," J. Lubr. Technol. 98 (2), 223-229.

Hamrock, B. J. and Dowson, D. (1977a) "Isothermal Elastohydrodynamic Lubrication of Point Contacts. Part IV - Starvation Results," J. Lubr. Technol., 99 (1), 15-23.

Hamrock, B. J. and Dowson, D. (1977b) "Isothermal Elastohydrodynamic Lubrication of Point Contacts. Part III - Fully Flooded Results," J. Lubr. Technol. 99 (2), 264-276.

Hamrock, B. J. and Dowson, D. (1978) "Elastohydrodynamic Lubrication of Elliptical Contacts for Materials of Low Elastic Modulus. Part I - Fully Flooded Conjunction," J. Lubr. Technol., 100 (2), 236-245.

Hamrock, B. J. and Dowson, D. (1979) "Elastohydrodynamic Lubrication of Elliptical Contacts for Materials of Low Elastic Modulus. Part II - Starved Conjunction," J. Lubr. Technol., 101 (1), 92-98.

Moes, H. (1965-66) "Communication, Elastohydrodynamic Lubrication," Proc. Inst. Mech. Engr., London, Part 3B, 180, 244-245.

Sanborn, D. M. (1969) "An Experimental Investigation of the Elastohydrodynamic Lubrication of Point Contacts in Pure Sliding," Ph. D. Thesis, University of Michigan.

Theyse, F. H. (1966) "Some Aspects of the Influence of Hydrodynamic Film Formation on the Contact Between Rolling/Sliding Surfaces," Wear, 9, 41-59.

Wedeven, L. E., Evans, D., and Cameron, A. (1971) "Optical Analysis of Ball-Bearing Starvation," J. Lubr. Technol., 93 (3), 349.

Wolveridge, P. E., Baglin, K. P., and Archard, J. G. (1971) "The Starved Lubrication of Cylinders in Line Contact," Proc. Inst. Mech. Eng. (London), 185 (1), 1159-1169.

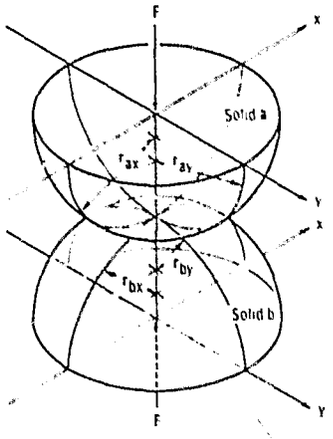

Figure 1. - Geometry of contacting elastic solids.

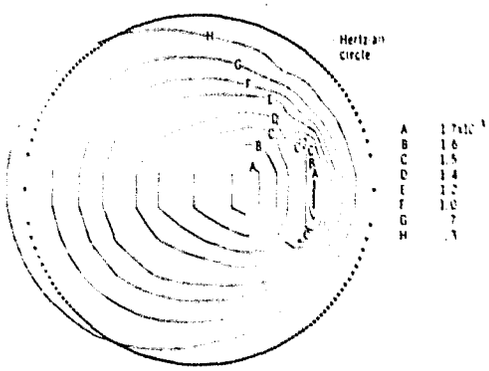

Figure 2. - Contour plot of dimensionless pressure. L = 1.25, U = 0.168x10^{-11}, W = 0.111x10^{-6}, and G = 4522.

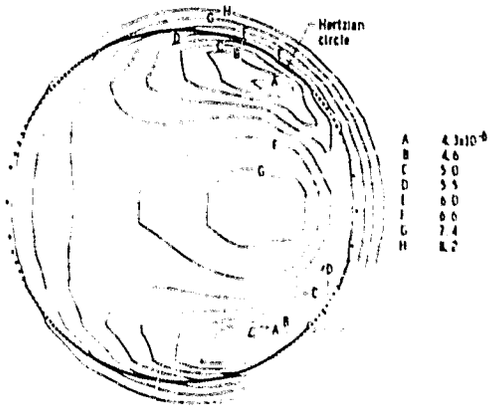

Figure 3. - Contour plot of dimensionless film thickness, $k = 1.25$, $U = 0.166 \times 10^{-11}$, $W = 0.111 \times 10^{-6}$, and $G = 4522$.

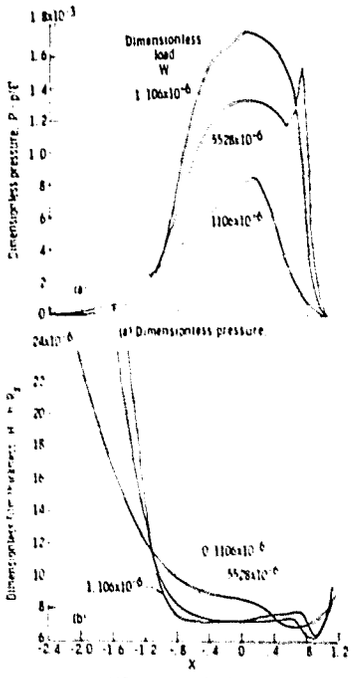

Figure 5. - Variation of dimensionless pressure and film thickness on X-axis for three values of dimensionless load parameter. The value of Y is held fixed near axial center of contact.

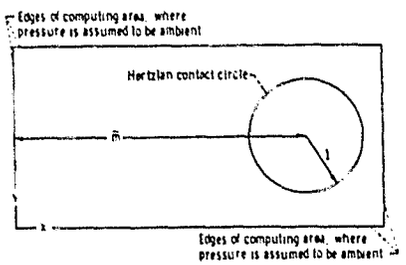

Figure 7. - Computing area in and around Hertzian contact zone.

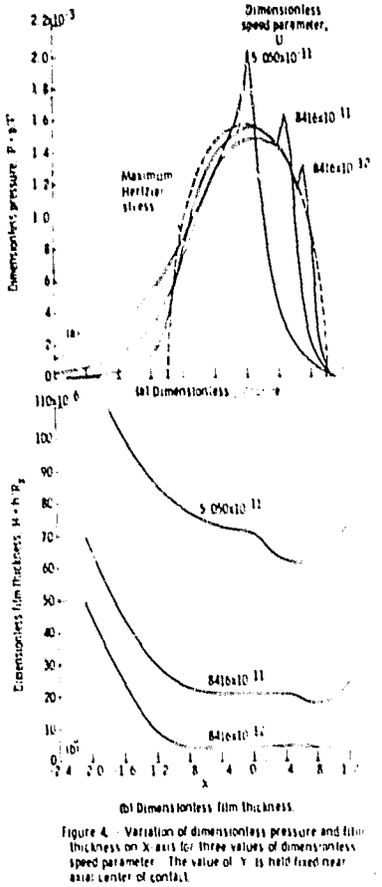

Figure 4. - Variation of dimensionless pressure and film thickness on X-axis for three values of dimensionless speed parameter. The value of Y is held fixed near axial center of contact.

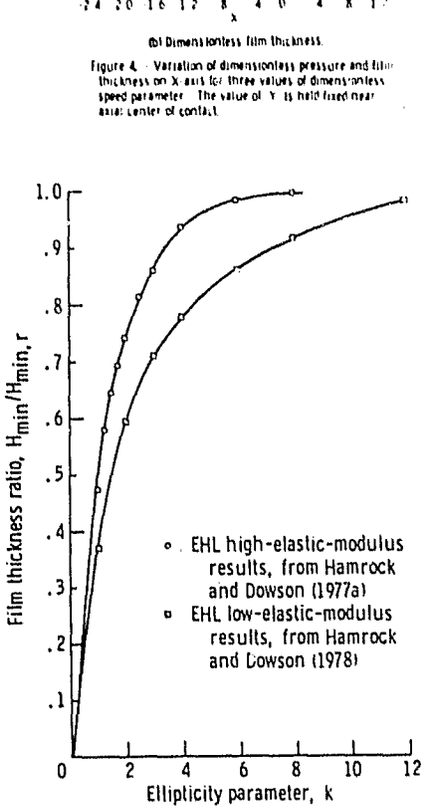

Figure 6. - Effect of ellipticity parameter on ratio of dimensionless minimum film thickness to dimensionless minimum film thickness for a line contact, for EHL high- and low-elastic-modulus analyses.

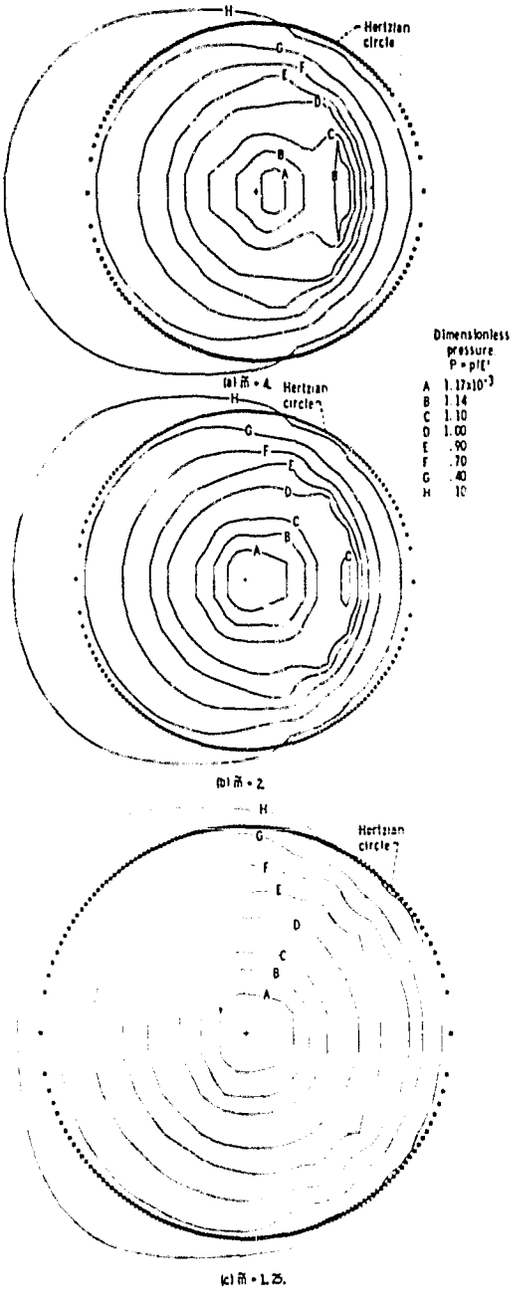

Figure 8. - Contour plots of dimensionless pressure for dimensionless inlet distances $\bar{m}$ of 4, 2, and 1.25 and for group 1 of table III.

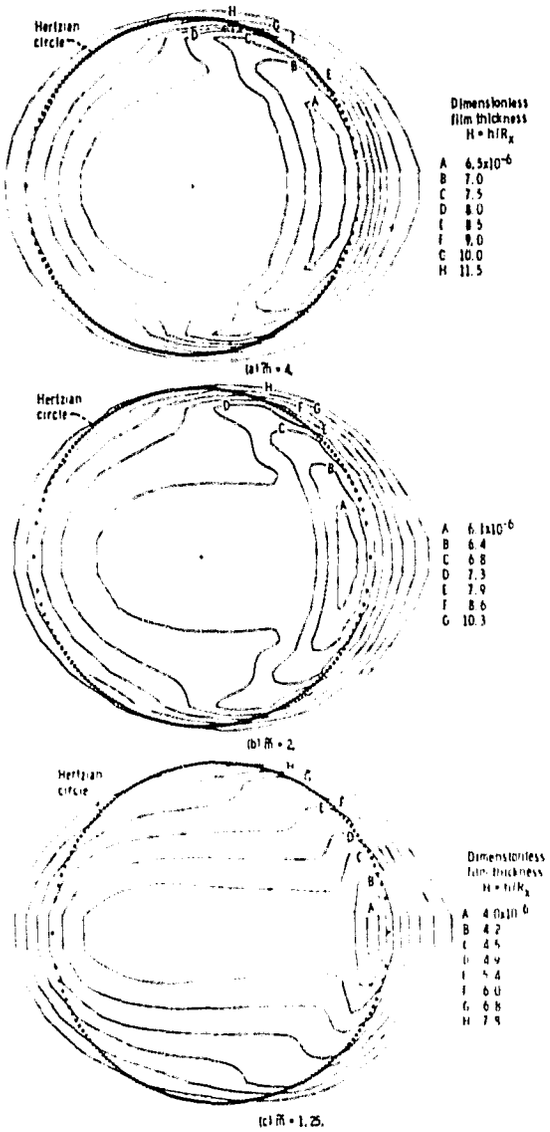

Figure 9. - Contour plots of dimensionless film thickness for dimensionless inlet distances $\bar{m}$ of 4, 2, and 1.25 and for group 1 of table III.

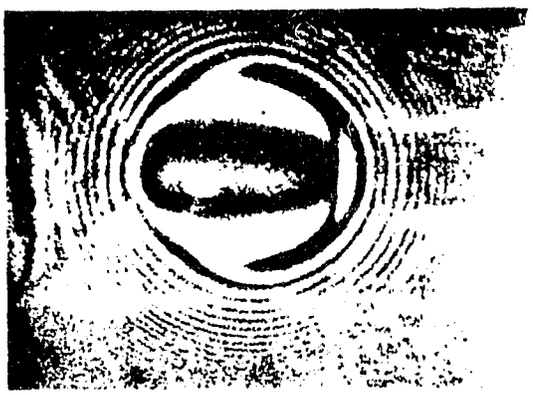

Figure 10. - Interference pattern for a starved elastohydrodynamic lubricated conjunction. (From Sanborn, 1969.)

TABLE I. - DATA SHOWING EFFECT OF ELLIPTICITY, LOAD, SPEED, AND MATERIALS PARAMETERS ON MINIMUM FILM THICKNESS FOR HARD EHL CONTACTS

Case	Ellipticity parameter, k	Dimensionless load parameter, W	Dimensionless speed parameter, U	Dimensionless materials parameter, G	Minimum film thickness		Difference between H_{min} and H_{min} D_1, percent	Results
					Obtained from EHL elliptical contact theory, H_{min}	Obtained from least-squares fit, H_{min}		
1	1	0.1106x10^{-6}	0.1683x10^{-11}	4522	5.143x10^{-6}	4.914x10^{-6}	+4.37	Ellipticity
2	1.25				4.895	4.898	-.06	
3	1.5				4.952	4.954	-.04	
4	1.75				4.952	4.955	+.08	
5	2				5.290	5.294	+.74	
6	2.5				5.756	5.801	+1.65	
7	3				6.091	6.196	-1.72	
8	4				6.636	6.636	-.00	
9	6				6.949	7.001	+.46	
10	8				7.048	7.091	+.61	
11	6	0.2211	0.1683x10^{-11}	4522	6.496	6.656	+2.53	Load plus case 9
12		.3866			6.317	6.412	+1.50	
13		.5528			6.268	6.225	-.69	
14		.7371			6.156	6.095	-.99	
15		.9214			6.088	5.997	-1.45	
16		1.106			5.811	5.918	+1.84	
17		1.290			5.857	5.851	+.43	
18	6	0.7371	0.08416	4522	3.926	3.805	-3.08	Speed plus case 14
19			.2525		8.372	8.032	-4.06	
20			.3367		9.995	9.769	-2.26	
21			.4208		11.61	11.37	-2.07	
22			.5892		14.39	14.29	-.69	
23			.8418		18.34	18.21	-.71	
24			1.263		24.47	24.00	-1.92	
25			1.683		29.75	29.18	-1.92	
26			2.104		34.58	33.96	-1.79	
27			2.525		39.73	38.44	-3.25	
28			2.946		43.47	42.69	-1.79	
29			3.367		47.32	46.76	-1.18	
30			4.208		54.57	54.41	-.29	
31			5.050		61.32	61.59	+.44	
32	6	0.7216	0.3296	2310	6.931	6.938	+0.10	Materials plus case 9
33	6	.7216	.9422	3491	17.19	17.59	+2.33	
34	6	.7456	.1122	6785	6.080	6.116	+.59	

TABLE II. - DATA SHOWING EFFECT OF ELLIPTICITY, LOAD, SPEED, AND MATERIALS PARAMETERS ON MINIMUM FILM THICKNESS FOR SOFT EHL CONTACTS

Case	Ellipticity parameter, k	Dimensionless load parameter, W	Dimensionless speed parameter, U	Dimensionless materials parameter, G	Minimum film thickness		Difference between H_{min} and H_{min} D_1, percent	Results
					Obtained from EHL elliptical contact theory, H_{min}	Obtained from least-squares fit, H_{min}		
1	1	0.4405x10^{-3}	0.1028x10^{-7}	0.4276	88.51x10^{-6}	91.08x10^{-6}	+2.90	Ellipticity
2	2				142.5	131.2	-7.93	
3	3				170.4	160.8	-5.63	
4	4				186.7	182.4	-2.30	
5	6				206.2	209.8	+1.75	
6	8				219.7	224.6	+2.23	
7	12				235.2	236.0	+.34	
8	6	0.4405x10^{-3}	0.05139	0.4276	131.8	133.7	+1.44	Speed plus case 5
9			.1542		268.1	273.1	+1.86	
10			.2570		381.6	380.7	-.24	
11			.05139		584.7	597.3	+2.15	
12	6	.2202	0.1028	0.4276	241.8	242.7	+0.37	Load plus case 5
13		.6607			190.7	192.7	+1.05	
14		1.101			170.5	173.1	+1.54	
15		1.542			160.4	161.3	+.56	
16		2.202			149.8	149.7	-.07	
17	6	0.1762	0.06169	1.069	181.8	182.5	+0.39	Material

TABLE III - EFFECT OF STARVATION ON MINIMUM FILM THICKNESS FOR HARD-EHL CONTACTS

Dimensionless Inlet Distance, $\tilde{m}$	Group 1	Group 2	Group 3
	Dimensionless Load Parameter, W		
	0.3686×10^{-6}	0.7371×10^{-6}	0.7371×10^{-6}
	Dimensionless Speed Parameter, U		
	0.1683×10^{-11}	1.683×10^{-11}	5.050×10^{-11}
	Minimum Film Thickness, H_{min}		
6	----------	29.75×10^{-6}	61.32×10^{-6}
4	6.317×10^{-6}	29.27	57.60
3	6.261	27.84	51.70
2.5	----------	26.38	46.80
2	5.987	23.46	39.91
1.75	----------	21.02	34.61
1.5	5.236	----------	27.90
1.25	3.945	----------	----------

TABLE IV - EFFECT OF DIMENSIONLESS SPEED AND LOAD PARAMETERS ON DIMENSIONLESS INLET DISTANCE AT FULLY FLOODED - STARVED BOUNDARY FOR HARD-EHL CONTACTS

Group	Dimensionless Parameters U	W	$R_x b$	Fully Flooded Film Thickness, Central, H_c	Minimum, H_{min}	Dimensionless Inlet Boundary, $\tilde{m}^*$
1	0.1683×10^{-11}	0.3686×10^{-6}	20.9	7.480×10^{-6}	4.211×10^{-6}	2.62
2	1.683	.7371	161.5	31.55	29.29	3.71
3	5.050	.7371	161.5	70.67	60.92	5.57

TABLE V - EFFECT OF DIMENSIONLESS INLET DISTANCE ON DIMENSIONLESS CENTRAL- AND MINIMUM-FILM-THICKNESS RATIOS FOR HARD-EHL CONTACTS

Group	Dimensionless Inlet Distance, $\tilde{m}$	Film Thickness Ratios for Starved and Flooded Conditions: Central, $H_{c,s}/H_c$	Minimum, $H_{min,s}/H_{min}$	Inlet Boundary Parameters: Critical, $\frac{\tilde{m}-1}{m^*-1}$	Wedeven, et al. (1971), $\frac{\tilde{m}-1}{m_W-1}$
1	2.62	1	1	1	0.9895
	2	.9430	.9640	.6173	.6108
	1.5	.7697	.8417	.3086	.3054
	1.25	.5689	.6341	.1543	.1527
2	3.71	1	1	1	0.8281
	2	.9574	.9534	.7380	.6111
	2.5	.8870	.9034	.5525	.4584
	2	.7705	.8034	.3690	.3056
	1.75	.7151	.7199	.2768	.2292
3	5.57	1	1	1	0.8498
	4	.9348	.9439	.6565	.5579
	3	.8330	.8487	.4376	.3719
	2.5	.7440	.7697	.3282	.2789
	2	.5223	.6551	.2188	.1860
	1.75	.5309	.5681	.1641	.1395
	1.5	.4155	.4580	.1094	.0930

TABLE VI - EFFECT OF STARVATION ON FILM THICKNESS FOR SOFT-EHL CONTACTS

Dimensionless Inlet Distance, $\tilde{m}$	Group 1	Group 2	Group 3
	Dimensionless Load Parameter, W		
	0.4405×10^{-3}	0.2202×10^{-3}	0.4405×10^{-3}
	Dimensionless Speed Parameter, U		
	0.5139×10^{-8}	0.1027×10^{-7}	0.5139×10^{-7}
	Dimensionless Minimum Film Thickness, H_{min}		
1.667	131.8×10^{-6}	241.6×10^{-6}	584.7×10^{-6}
1.633	131.2	238.6	572.0
1.667	120.7	230.8	543.1
1.500	125.6	217.2	503.0
1.333	115.9	190.3	444.0
1.167	98.11	120.8	272.3
1.033	71.80	120.6	272.3

TABLE VII - EFFECT OF INLET DISTANCE ON FILM THICKNESS FOR SOFT-EHL CONTACTS

Group	Dimensionless Parameters U	W	$R_x b$	Fully Flooded Minimum Film Thickness, H_{min}	Dimensionless Inlet Boundary, $\tilde{m}^*$
1	0.5139×10^{-8}	0.4405×10^{-3}	19.41	127.8×10^{-6}	1.661
2	$.1027\times10^{-7}$	.2202	24.45	238.5	1.757
3	.5139	.4405	19.41	567.2	1.850

TABLE VIII - EFFECT OF INLET DISTANCE ON MINIMUM FILM-THICKNESS RATIO FOR SOFT-EHL CONTACTS

Group	Dimensionless Inlet Distance, $\tilde{m}$	Ratio of Minimum Film Thicknesses for Starved and Flooded Conditions, $H_{min,s}/H_{min}$	Critical Inlet Boundary Parameter, $(\tilde{m}-1)/(m^*-1)$
1	1.661	1	1
	1.500	.9928	.7564
	1.333	.9069	.5038
	1.167	.7677	.2526
	1.033	.5616	.0499
2	1.757	1	1
	1.667	.9642	.8811
	1.500	.8262	.6605
	1.333	.6499	.4399
	1.167	.7267	.2206
	1.033	.5151	.0436
3	1.850	1	1
	1.667	.9575	.7847
	1.500	.8868	.5882
	1.333	.7844	.3918
	1.167	.6761	.1965
	1.033	.4801	.0388